International Journal for Parasitology: Drugs and Drug Resistance 7 (2017) 337–349

Contents lists available at ScienceDirect

International Journal for Parasitology: Drugs and Drug Resistance

journal homepage: www.elsevier.com/locate/ijpddr

L-Asparaginase of *Leishmania donovani*: Metabolic target and its role in Amphotericin B resistance

Jasdeep Singh [a], Mohd Imran Khan [b, 1], Shiv Pratap Singh Yadav [c, 1], Ankit Srivastava [a], Kislay K. Sinha [b], Ashish [c], Pradeep Das [d], Bishwajit Kundu [a, *]

[a] Kusuma School of Biological Sciences, Indian Institute of Technology Delhi, New Delhi 110016, India
[b] National Institute of Pharmaceutical Education & Research, EPIP Complex, Hajipur, Vaishali 844102, India
[c] The Council of Scientific and Industrial Research Institute of Microbial Technology, Chandigarh, India
[d] Rajendra Memorial Research Institute of Medical Sciences, Patna 800007, India

ARTICLE INFO

Article history:
Received 19 May 2017
Received in revised form
22 August 2017
Accepted 21 September 2017
Available online 28 September 2017

Keywords:
Leishmania donovani
L-asparaginase
Amphotericin B resistance
Metabolic target

ABSTRACT

Emergence of Amphotericin B (AmB) resistant *Leishmania donovani* has posed major therapeutic challenge against the parasite. Consequently, combination therapy aimed at multiple molecular targets, based on proteome wise network analysis has been recommended. In this regard we had earlier identified and proposed L-asparaginase of *Leishmania donovani* (LdAI) as a crucial metabolic target. Here we report that both LdAI overexpressing axenic amastigote and promastigote forms of *L. donovani* survives better when challenged with AmB as compared to wild type strain. Conversely, qRT-PCR analysis showed an upregulation of LdAI in both forms upon AmB treatment. Our data demonstrates the importance of LdAI in imparting immediate protective response to the parasite upon AmB treatment. In the absence of structural and functional information, we modeled LdAI and validated its solution structure through small angle X-ray scattering (SAXS) analysis. We identified its specific inhibitors through ligand and structure-based approach and characterized their effects on enzymatic properties (K_m, V_{max}, K_{cat}) of LdAI. We show that in presence of two of the inhibitors L1 and L2, the survival of *L. donovani* is compromised whereas overexpression of LdAI in these cells restores viability. Taken together, our results conclusively prove that LdAI is a crucial metabolic enzyme conferring early counter measure against AmB treatment by *Leishmania*.

1. Introduction

Leishmaniasis, caused by protozoan parasite *Leishmania* manifests into three major clinical forms, cutaneous, mucocutaneous and visceral which is usually but not exclusively species specific (Desjeux, 2004). Considering all forms, the disease is prevalent in 98 countries with estimated 1.3 million new cases worldwide (Alvar et al., 2012). However, the major death toll (20000–30000 deaths per year) results mainly from visceral leishmaniasis (Kala-azar) caused by *Leishmania donovani* and is predominantly endemic in the East Africa and Indian subcontinent (Alvar et al., 2012). Due to high morbidity rates and rapidly developing drug resistance, the parasite causes socio-economic loss and accounts to ninth largest disease burden among all infectious diseases (Chakravarty and Sundar, 2010; Croft et al., 2006; Alvar et al., 2012). Shortcomings of current line therapies for the disease pose challenges in developing novel anti-microbial only in leishmaniasis but also other parasites infecting humans. This calls for exploring newer and potent drug targets with clear understanding of the molecular basis of drug resistance (Chandra and Puri, 2015, Gilleard and Beech, 2007; Mateos-Gonzalez et al., 2015; Venkatesan and Borrmann, 2015; Saunders et al., 2013). *Leishmania* exhibits a digenetic life cycle as promastigotes in insects and amastigotes in mammals (Tsigankov et al., 2014). Upon infecting the host this protozoan resides inside the hostile environment of macrophages and differentially expresses wide array of proteins for survival (Naderer and Mcconville, 2011, Morales et al., 2008, 2010; Casgrain et al., 2016; Cull et al., 2014). Enzymes involved in energy metabolism and defense strategies such as suppression and evasion of host immune responses are primarily implicated in survival mechanisms (Mcconville, 2016; Mcconville and Naderer, 2011).

* Corresponding author.
E-mail address: bkundu@bioschool.iitd.ac.in (B. Kundu).
[1] The authors have equal contributions.

https://doi.org/10.1016/j.ijpddr.2017.09.003

Asparagine/glutamine related metabolic pathways in *Leishmania* had been subject of recent interest to understand their role in maintaining cellular homeostasis (Faria et al., 2016; Nowicki and Cazzulo, 2008; Manhas et al., 2014). For instance, aspartate uptake has been proved crucial in TCA cycle anaplerosis of *Leishmania mexicana* and glutamate as metabolic precursor for other pathways (Saunders et al., 2011; Nowicki and Cazzulo, 2008). More recently, through reconstructed energy metabolism network of *Leishmania infantum,* glutamate biosynthesis has been implicated as a crucial target against the parasite (Faria et al., 2016; Moreno et al., 2014). In many related pathogens such as *Salmonella typhi, Helicobacter pylori* etc. also, which need to survive under harsh acidic conditions inside host, Asn/Gln metabolism has been proved to be important for cellular survival, host invasion, mediation of virulence and host immunity (Scotti et al., 2010; Kullas et al., 2012; Shibayama et al., 2011). Interestingly, *Leishmania* manages to carry its digenetic life cycle by maintaining a neutral intracellular pH, in spite of acidic extracellular environment posed by the host macrophage (Zilberstein et al., 1991). Naturally, any tinkering with this pH difference across parasite's membrane will be detrimental for its survival. In this line, exposure to membrane altering agents such as polyene antibiotic Amphotericin B (AmB) has been successful in treating this parasite. AmB interacts with ergosterol within the membrane, altering its permeability through the formation of non-aqueous and aqueous pores resulting in positive K^+/H^+ gradient (Palacios and Serrano, 1978; Jiang et al., 1994; Herec et al., 2005; Cohen, 2010; Saha et al., 1986; Luque-Ortega et al., 2003). This in turn follows a caspase-3 dependent apoptosis of the pathogen (Saha et al., 1986; Cohen, 2010). Additionally, this antibiotic is known to exhibit immunomodulatory effects and foster parasitic clearance by stimulating the transcription and production of proinflammatory cytokines like TNF-α, IL-1β, MCP-1, MIP-1β, nitric oxide, prostaglandins and intercellular adhesion molecule-1 from murine and human immune cells (Mesa-Arango et al., 2012; Sau et al., 2003). This occurs via signaling molecules as Toll like receptor (TLR)-2, Bruton's tyrosine kinase (Btk) and phospholipase C (PLC) (Arning et al., 1995; Matsuo et al., 2006; Bellocchio et al., 2005; Mihu et al., 2014). Further AmB mediates induction of free radicals which in turn is linked to protein kinase C (PKC) (Mukherjee et al., 2010). Interestingly, the immediate countermeasures adopted by *L. donovani* to reduce pH imbalance inflicted by AmB have not been extensively studied. One defensive mechanism could be the over-expression of surface P-type K^+, H^+-ATPase, normally expressed in parasites for expelling protons by nutrient mediated symport (Jiang et al., 1994; Anderson and Mukkada, 1994). However, studies on AmB resistance by Brotherton et al. proposed against over-expression of K^+, H^+-ATPase, as this coutermeasure could result in unnecessary depletion of ATP in the parasite, already in stressed state (Brotherton et al., 2014). Therefore, to maintain a neutral intracellular environment in such conditions, an ATP independent mechanism should be ideally operating to neutralize H^+ gradient.

We hypothesize that the L-asparaginase (LdAI) of *Leishmania donovani* may be a crucial metabolic enzyme rendering immediate protection or defense to parasite on exposure to AmB. Our hypothesis is based on the fact that ammonia (NH^{4+}), released by the action of LdAI amidohydrolase on Asn/Gln, could be involved in counteracting the acid influx (acid stress) mediated by AmB induced membrane pore formation. Our hypothesis is supported by studies on a similar L-asparaginase of *Mycobacterium tuberculosis* where the ammonia released aids in its survival inside acidic environment of human alveolar macrophages (Gouzy et al., 2014). Likewise, *E. coli* exploits similar survival mechanism to resist environmental acidic stress by enzymatic release of ammonia through glutaminase (Lu et al., 2013).

Our hypothesis was validated when LdAI transfected strains of both promastigote and axenic amastigotes of *Leishmania donovani* showed increased tolerance and better survival against AmB compared to wild type strains. Retrospectively, LdAI upregulation was observed in both forms upon AmB treatment, supporting the fact that LdAI is conferring survival advantage to these AmB challenged parasites. We further characterized LdAI structurally and functionally. Earlier we had modeled the structure of this enzyme and proposed potential inhibitors, L1 and L2 (Singh et al., 2015). In this study we report that these inhibitors (albeit at high concentrations but non-toxic to humans) could effectively retard the growth of *Leishmania* indicating necessity of LdAI to the parasite. Overall this study on LdAI provides direct experimental evidence of its metabolic importance in *L. donovani* survival which had been overlooked in earlier genome wide network analysis. Although pathways for Asp/Glu production may exhibit redundancy, nonetheless the findings reveal new and additional functional measure taken by the parasite in counteracting drug effects.

2. Materials and methods

2.1. Construction of LdAI expression vectors and its transfection in L. donovani

The LdAI gene was PCR amplified from *L. donovani* genome using primer pairs 5′ TTTTAAGCTTACAATGGAAGCGGGAATAGAGG 3′ and 5′ TTTTCTCGAGTCACAGCTTCGCATGCACTTCG 3′ containing restriction sites *Hin*dIII and *Xho*I (underlined), respectively. The amplified product was cloned into pLpneo2 for expression in *Leishmania*. Positive clones were verified by sequencing. *L. donovani* AG83 cells were transfected with clone or empty vector using electroporation following the high-voltage protocol described by Robinson and Beverley (Beverley and Clayton, 1993). Transfectants were selected and maintained in the presence of G418 (100 μg/ml). RT PCR was used to verify the transcription of the cloned gene (as discussed in Section 2.3.2).

2.2. Survival of wild type and LdAI over-expressing parasites upon treatment with Amphotericin B and inhibitors L1 and L2

L. donovani wild type AG83 (WT) and pLP2-LdAI transfected promastigotes (WT-LdAI) were maintained in M199 medium (pH 5.5) containing 10% FBS as described. The late exponential phase parasites were appropriately diluted (2×10^6 promastigotes/ml) and treated with varying concentrations of Amphotericin B and previously screened inhibitors L1 and L2, prepared in M199 medium lacking FBS. Similarly, for testing chemosusceptiblity of wild type (WT) and LdAI transfected amastigotes (WT-LdAI) to AmB, axenically grown amastigotes were used as established in protocol by Sereno D et al. (Sereno and Lemesre, 1997). Parasite viability was evaluated using the quantitative colorimetric MTT assay where OD was measured at 570 nm by using micro plate reader. IC_{50} was defined as the concentration that reduced parasite survival by 50%. The results are expressed as % survival with mean and standard error from three independent experiments. IC_{50} of each compound and AmB was calculated by fitting the data into Dose-response (log (inhibitor) vs. normalized response) equation using GraphPad Prism 5:

$$Y = \frac{100}{1 + 10^{(X - LogIC50)}}$$

where IC_{50} is the concentration that gives response intermediate between the maximum and the minimum.

Further, IC_{90} calculated from IC_{50} using following equation:

$$IC90 = F - (100 - F)^{\frac{1}{H}} \cdot IC50$$

where H is hill slope and F is fraction of maximal response.

2.3. RNA isolation from L. donovani strain

Isolation of total RNA from *L. donovani* was performed by using TRIZOL method; 1 ml (5×10^7/ml) cultured cells were pelleted down by centrifugation (4500 g for 10 min), washed with PBS and then mixed with TRIZOL solution and allowed to stand at room temperature for 5 min. Following this 0.2 ml of chloroform (100%) was added; mixture was shaken vigorously for 15 s and incubated at room temperature for 3 min. Three distinct layers came out after centrifugation at 12,000*g* for 15 min at 4 °C, 80% of top layer was taken in fresh tube and 0.5 ml of isopropyl alcohol (100%) was added then incubated at room temperature for 10 min. Contents were centrifuged at 12,000 *g* for 10 min at 4 °C, supernatant was discarded and 1 ml of 75% chilled ethanol was added, vortexed and centrifuged at 7500 g for 5 min at 4 °C. Ethanol was removed carefully and it was air dried for 5 min. The RNA pellet was dissolved in double distilled RNase free water. Quality of RNA was checked by gel electrophoresis and quantified by Nanodrop spectrophotometer (Thermo scientific, Nanodrop 2000; USA).

2.3.1. cDNA synthesis

The reverse transcription of 200 μg of total RNA was performed using Transcriptor High Fidelity cDNA synthesis kit as per manufacturer's instructions. The cDNA was quantified spectrophotometrically and used for subsequent amplifications.

2.3.2. Semi quantitative RT-PCR and real-time PCR

Reverse transcription was performed using 200 μg total RNA from *L. donovani* cells treated with 0.125 μg/ml AmB- for 8 h and untreated cells as control. The cDNA from *L. donovani* treated identically were PCR amplified with gene-specific primers for LdAI and alpha tubulin. The products were quantified on 2% agarose gel using Quantity One software. All the reverse transcription PCR (RT-PCR) products were normalized with respect to the alpha-tubulin. These semiquantitative data were validated by quantitative real-time PCR (BIO-RAD) using SYBR green (Thermo scientific). Sequences of the primers used: 5′-GTTGCGCACAAGCACAATA-3' (forward) and 5′-GTCGTTCAGGTACACGATCTC-3' (reverse) for LdAI and 5′-ATGCCAAGTGACAAGACCATTGGG-3' (forward) and 5′-TTATTGGCAGCATCCTCCTTGCCT-3' (reverse) for α-tubulin.

2.4. Multiple sequence alignment and STRING analysis

To determine identity and conservation of residues in the catalytic triads of different asparaginases belonging to enteric pathogens, multiple sequence alignment of various L-asparaginases from *L. donovani* (UNIPROT E9BC85), *H. pylori, M. tuberculosis* and human L-asparaginase was done using CLUSTAL Omega. 3D structure alignment of LdAI with L-asparaginase of *M. tuberculosis* and *S. typhi* (pre-available at Protein Model Portal at Protein Structure Initiative Knowledgebase (PSI KB)) and *H. pylori* (PDB id: 2WLT) was done using PyMol. For identifying potential interaction partners, STRING (Von mering et al., 2005) analysis was done for LdAI and predicted functional partners with confidence score of ≥ 0.9 were retained.

2.5. Purification and structural characterization of LdAI

2.5.1. Purification

LdAI was also PCR amplified and cloned between *Hin*dIII and *Xho*I restriction sites of *E. coli* expression plasmid pET 28a (Novagen) with forward (5′ TTTTAAGCTTACAATGGAAGCGGGAATAGAGG-3′) and reverse (5′ TTTTCTCGAGTCACAGCTTCGCATGCACTTCG-3′) primers. Following confirmation of positive clones by DNA sequencing, *E. coli* BL21 DE3 expression host was transformed with the pET construct and cells were grown in LB medium (HiMedia Corp.) with 100 μM kanamycin (Biobasic Inc.). Induction was done using 1 mM IPTG (Biobasic Inc.) at 0.6–0.7 OD_{600}, followed by growth for 16 h at 18 °C and culture harvesting by centrifugation at 6000*g*. Cell pellet was lysed by sonication in 50 mM Tris 500 mM NaCl pH 8.0 buffer with 10 mM imidazole and 10% glycerol. Sonicated lysate was again centrifuged for 1 h at 16,000 g followed by loading of the supernatant to pre-equilibrated Ni-NTA column (GE Healthcare) connected to ÄKTA purifier FPLC system (GE Healthcare). Protein was eluted by applying linear gradient of 50–500 mM imidazole within the same buffer. The peak corresponding to the protein of interest was collected and dialyzed against 10 mM Tris 100 mM NaCl pH 8.0 for further processing through size exclusion chromatography. The dialyzed sample was concentrated and centrifuged before loading to Superdex 200 (10/300 GL, GE Healthcare) column. Because of absence of tryptophan residues in LdAI, protein concentrations were measured at A_{274} corresponding to absorption of Tyr using molar extinction coefficient of 21,360 $M^{-1}cm^{-1}$ (ProtParam).

2.5.2. Structural characterization

Multimeric nature of LdAI was assessed through size exclusion Chromatography (GE Healthcare) and Small Angle X-ray Scattering. Filtered protein solution (10 μg) was centrifuged at 14 k rpm for 20 min to remove soluble aggregates followed by loading on a Superdex 200 analytical gel filtration column (10/300 GL; GE Healthcare) and eluted with column equilibration buffer (10 mM Tris 100 mM NaCl, pH 8.0). SAXS data for wild type LdAI was collected at *in-house* SAXSpace instrument with a sealed tube source (Anton Paar, Graz, Austria). All experiments were done using line collimation and scattered X-rays were detected on CMOS Mythen detector (Solanki et al., 2014; Wagner et al., 2016). Purity and homogeneity of protein samples (SEC purified) were confirmed by single bands near the expected migration position on 12% SDS-PAGE, prior to SAXS data collection. Dialysis was performed to remove imidazole and to reduce the salt concentration, last dialysis buffer was used as match buffer for SAXS data collection. Samples were again centrifuged at 14 K to remove any soluble aggregates. For each data acquisition 50 μl sample of LdAI and the matched (last dialysis) buffer were exposed for 1 h at 20 °C temperature in a thermostated quartz capillary of 1 mm diameter. SAXStreat program was used for data reduction and to calibrate the position of primary beam. SAXSquant software was further used for buffer subtraction and desmearing of all the samples to obtain intensity profiles. The desmeared I(Q) files obtained from SAXSquant software was further analyzed by SAS data analysis of ATSAS 2.8.2 suite (Petoukhov et al., 2012). Radius of gyration function was used for Guinier analysis assuming globular (R_g) and rod (R_c), keeping Guinier approximations in mind. Distance distribution function of the SAS data analysis was used to compute the maximum linear dimension of the protein (D_{max}) which uses indirect Fourier transformation to calculate the pair wise distribution function of all the inter-atomic vectors, *P(r)*. Probability of finding vector equal to 0 nm and maximum linear dimension of scattering particles was considered to be zero. DAMMIF(Franke and Svergun, 2009), software was further used to generate 10 independent uniform density

models which were aligned and averaged to obtain predominant scattering shape of particles. DAMCLUST program was further used to compare all the models on the basis of NSD values. This model was further refined using DAMMIN program to be compared with theoretical structure of protein using template crystal structure (PDB id: 4Q0M). SUPCOMB program was used for automated alignment of models which aligns inertial axes in three dimensions.

2.6. Specific activity assessments and kinetic analysis

Specific asparaginase and glutaminase activity at pH 8.0 was determined by standard Nesslerization protocol described elsewhere (Bansal et al., 2010). For determination of kinetic constants, K_m and K_{cat}/K_m (catalytic efficiency), steady state enzyme kinetics were monitored in 20 mM Tris 150 mM NaCl, pH 8.0 at 298 K using constant LdAI and varying concentration of substrates (0–80 mM).

2.7. Fluorescence measurements

2.7.1. Association of inhibitors with LdAI

K_d (dissociation constant) determination for affinity of screened ligands L1 and L2 with LdAI was calculated by both Fluorescence Spectroscopy and Isothermal Titration Calorimetry (ITC). In all cases, experiments were carried in 20 mM Tris 150 mM NaCl, pH 8.0 at 298 K.

Fluorometric titrations were carried in Perkin Elmer LS55 spectrophotometer. At constant enzyme concentration of 2 μM, titrations were carried with increasing concentrations of L1 and L2 up to 5 μM with a pre scan delay of 300 s. Incubated samples were excited at 274 nm emission spectra were recorded from 290 nm to 400 nm. To determine K_d, fluorimetric titration data was fitted using single site specific binding module of GraphPad Prism v 5.0. The following equation was used for data:

$$Y = Bmax^{*}X / (K_d + X)$$

where Bmax is the maximum specific binding and X represents concentration of L1 and L2 at each titration.

2.7.2. Assessment of LdAI stabilization/destabilization by L1 and L2

Intrinsic Tyr fluorescence-based thermal shift (FTS) assay was done by monitoring change in Tyr emission at 330 nm over the temperature range from 25 to 90 °C with step size of 2 °C. Excitation and emission slits were kept at 5/10 with an equilibration time of 1 min at each step. Thermal denaturation of LdAI alone was done at the concentration of 2 μM while in the presence of ligands, 100 μM of L1 and L2 were pre-incubated with 2 μM of enzyme for 30 min prior to experiments.

2.8. Isothermal titration calorimetry studies

2.8.1. Thermodynamics of L1 and L2 association with LdAI

To obtain thermodynamics of L1 and L2 association with LdAI, ITC titrations were carried in Microcal VP-ITC (MicroCal Inc., USA). In all titrations, 3 μM of LdAI was loaded into cell and titrated against L1 and L2 (single injection of 1 μL followed by 25 injections of 4 μL from stock concentration of 120 μM in syringe). Buffer dilutions were carried in similar way to normalize heats of dilution. Single site binding model was used to analyze association of compounds with LdAI according to following equation:

$$A + M \leftrightharpoons AM$$

$$K_a = \frac{[AM]}{[A][M]}$$

Where M is macromolecule (LdAI) and A represents the ligands L1 or L2. K_a represents association constant of LdAI with the ligands. The resulting isotherms were then analyzed using Levenberg-Marquardt non-linear least squares curve fitting algorithm pre supplied with Origin 7.0 (Origin Lab corporation, USA) to obtain K_a (Association constant), ΔH (Enthalpy) and ΔS (Entropy). Free energy of binding was calculated according to equation:

$$\Delta G = \Delta H - T\Delta S$$

2.8.2. Competitive binding of inhibitors with LdAI

Due to spontaneous hydrolysis of L-asparagine/L-glutamine by LdAI their binding affinities could not be accurately determined. Previously, Jayaram HN et al. used L-aspartic acid to probe its interactions with L-asparaginase from *E. coli* and accurately determined dissociation constant in 60–160 μM range (Jayaram et al., 1986). In similar manner, we first determined association of L-aspartic and L-glutamic acid by fluorescence spectroscopy and ITC. Enzyme (3 μM) was loaded into ITC cell and titrated against 150 μM of L-aspartate/L-glutamate with constant stirring at 300 rpm.

Further, in order to study the association of ligands with LdAI in the presence of aspartate/glutamate, competitive binding experiments were carried using ITC(Sigurskjold, 2000). Single site fitting module was used to assess binding affinity of one ligand, when added to equilibrium mixture of LdAI and aspartate/glutamate as described below:

$$\begin{array}{ccc} M + A & \leftrightharpoons & MA \\ + & & + \\ B & & B \\ \Updownarrow & & \Updownarrow \\ MB + A & \leftrightharpoons & MAB \end{array}$$

where, M is macromolecule (LdAI) and A, B are competing ligands.

As above 3 μM of LdAI was pre-incubated with 60 μM of L-aspartate and L-glutamate for 30 min, which was titrated against 150 μM of L1 and L2 separately. Total concentration of competing ligand, $[B]_{total}$ is maintained in a way that:

$$\frac{K_A}{[B]_{total}\ K_B} = 10^5 - 10^8 M^1$$

Where A is strongly binding ligand to LdAI under study and B is competing ligand (may be aspartate or glutamate). K_A and K_B are the apparent association constants of A and B, respectively.

2.9. Competitive inhibition assays and specificity of L1 and L2 for LdAI

The ligands L1 and L2 were screened on the basis of their affinity with residues of the active site pocket of LdAI. Thus, competitive inhibition by these compounds can be monitored in terms of decline in specific activity due to inhibition of substrate hydrolysis at active site using standard Nesslerization protocol described above. Briefly, 2 μM of LdAI was pre incubated with saturating concentrations of L1 and L2 (100 μM each, pre-determined by ITC) and concentration of substrate was varied in each reaction mixture

to monitor change in specific activity. To ensure their specificity the inhibitors L1 and L2 selected against LdAI were also tested on other asparaginases viz. *Escherichia coli* (EcAII) and *Pyrococcus furiosus* (PfA). EcAII was purchased from Sigma Aldrich co. (USA) while PfA was purified according to previous protocols from our lab (Bansal et al., 2010). All reagents were procured from Sigma-Aldrich (otherwise stated) molecular biology grade. Both inhibitors were commercially synthesized from Vitas-M Laboratory, USA.

2.10. Molecular dynamics simulations

All simulations were carried using GROMACS 5.1(van der spoel et al., 2005) software package under charmm 27 force field (Sapay and Tieleman, 2011; Pentikainen et al., 2009). Structures of L1 and L2 were imported from PubChem Compound Database while the topology and other parameters were assigned using SwissParam (Zoete et al., 2011). To study the effect of L1 and L2 on LdAI, the compounds were docked onto its previously identified active sites and placed in individual cubical boxes with 15 Å edge spacing. LdAI alone was also setup similarly serving as control system along with appropriate amount ions added to maintain electro neutrality at 0.15 M NaCl. Energy minimization of the system was carried by steepest descent scheme followed by 1 ns equilibration using an isothermal-isobaric and isochoric-isothermal ensemble. Long range electrostatics were treated using PME and short range interactions at cutoff radius of 10 Å for both coulomb and van der Waal potentials. System temperature (310 K) and pressure (1 bar) was kept constant using velocity rescale and Berendsen barostat respectively. Velocities were generated by solving Newton's equations of motion and the coordinates were recorded at each 10 ps interval using 2 fs time step using Leap frog integrator. Trajectories were then analyzed using standard GROMACS tools.

3. Results

3.1. Role in AmB resistance

3.1.1. Early resistance to AmB by LdAI

Chemosusceptibility to frontline anti-leishmaniasis drug AmB was assessed on both wild type and LdAI overexpressing parasites. IC_{50}'s calculated from dose-response curves in wild type strains corroborated with previous studies on AmB toxicity to both promastigotes (0.6 ± 0.07 μM) and amastigotes (0.2 ± 0.0.05 μM) (Fig. 1A–B and Supplementary Table 1) (Sereno and Lemesre, 1997; van den bogaart et al., 2014). In contrast the LdAI transfected parasites showed moderate sensitivity to AmB as reflected through nearly three- and eight-fold increase in IC_{50} against promastigotes (2.2 ± 0.3 μM) and amastigotes (1.9 ± 0.6 μM) respectively, when compared to non-transfected strains (Supplementary Table 1). Interestingly, chemotolerance imparted by LdAI was not restricted to lower but also manifested at higher antibiotic concentrations. The wild-type strains were more susceptible at higher AmB concentrations than LdAI over-expressing parasites inferred through nearly three- and eight-fold lower IC_{90} against promastigote and amastigote forms respectively (Supplementary Table 1).

3.1.2. LdAI expression upon treatment with Amphotericin B

Since AmB toxicity was better tolerated by both LdAI over-expressing forms, we wanted to retro inspect whether the antibiotic exposure could modulate endogenous expression of LdAI in parasites. Semiquantitative PCR was first performed using cDNA preparations of AmB treated and untreated promastigotes which indicated 2.5 fold enhancement in LdAI transcription upon drug treatment (Supplementary Fig. 1). Subsequently, quantitative real time PCR analysis for both promastigotes and axenic amastigotes showed nearly four and five fold increase in LdAI transcript expression respectively (Fig. 1C).

3.2. Sequence alignment and structural features

L-asparaginase of *L. donovani* is a 398 amino acids long protein with a predicted molecular mass of 42.9 KDa. Modeled structure of LdAI dimer is shown in Fig. 2A. Multiple sequence alignment revealed similarity among the L-asparaginases (low E-scores) of intracellular pathogens like *S. typhi* (StA), *M. tuberculosis* (MtA) *and H. pylori* (HpA), each one of which survives under acidic environment inside the hosts (Fig. 2B). All these asparaginases displayed high degree of conservation in catalytic residues (>90% identity) as well as in their tertiary structural folds (Fig. 2B and C) with RMSD of 2.4 Å, 3.1 Å and 2.4 Å from HpA, MtA and StA respectively. In contrast, Human L-asparaginase (Type III) showed negligible sequence identity with LdAI which belongs to Type I family of L-asparaginases (cytoplasmic). In order to find out the interacting proteins of LdAI, STRING analysis was performed which yielded four strong interacting partners (confidence > 0.9) viz. aspartate aminotransferase, arginosuccinate synthase, adenonyl succinate synthase and asparate carbamoyltransferase (Fig. 2D).

3.3. Protein expression, purification and structural characterization

The recombinant LdAI was purified to >98% using affinity and

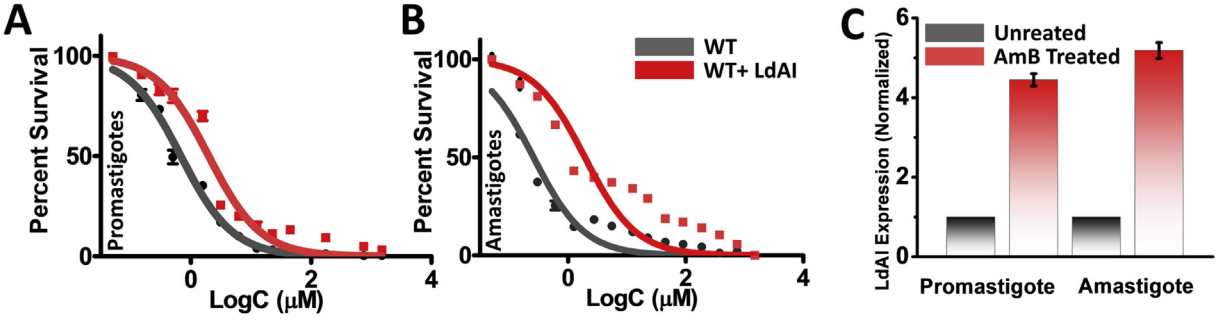

Fig. 1. AmB treatment of promastigotes and axenic amastigotes and its effect on endogenous LdAI expression. (A and B) Dose response curves of *L. donovani* promastigotes and axenic amastigotes to AmB. Normalized values are plotted as the means and standard errors from three replicates. (C) Quantitative real-time PCR analysis of expression levels of LdAI in AmB treated and untreated control promastigotes and axenically cultured amastigotes. Data are the ratios of target (LdAI)/reference (α-tubulin) shown as AmB untreated (Grey) versus treated (Red) cells. The -fold expression of each transcript was calculated using the $2^{-\Delta\Delta CT}$ method. The -fold expression in promastigotes and axenic amastigotes was plotted as means and standard deviation. (For interpretation of the references to colour in this figure legend, the reader is referred to the web version of this article.)

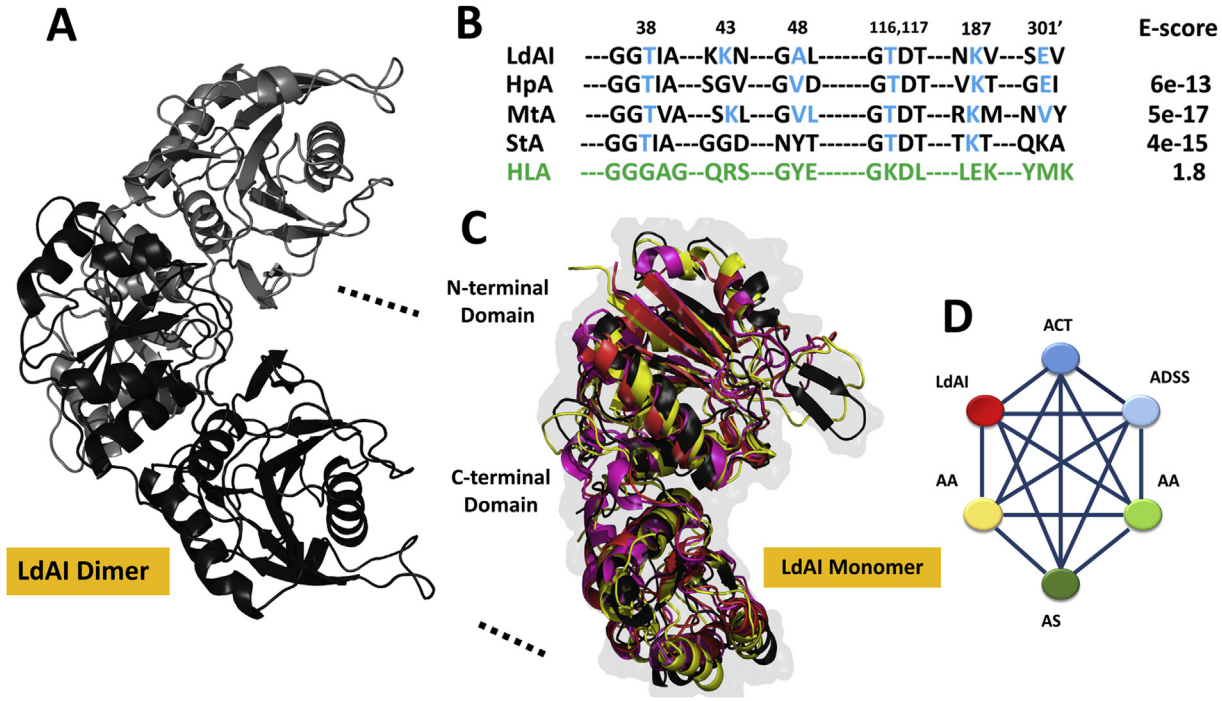

Fig. 2. Structural and sequence features of LdAI. (A) Modeled LdAI dimer with oppositely oriented monomers (Black and Grey) (B) Multiple sequence alignment of LdAI with HpA, MtA, StA and HLA. (C) LdAI monomeric unit showing its N- and C-terminal domains (Black) and aligned structurally with L-asparaginase of *H. pylori* (HpA, Yellow), *M tuberculosis* (MtA, Violet) and *S. typhi* (StA, Red). Both domains of LdAI orient oppositely to form active dimer. (D) STRING network analysis of LdAI within *L. donovani* showing most significant interacting partners (confidence > 0.9), aspartate aminotransferase (AA), arginosuccinate synthase (AS), adenonyl succinate synthase (ADSS) and asparate carbamoyltransferase (ACT). (For interpretation of the references to colour in this figure legend, the reader is referred to the web version of this article.)

size exclusion chromatography (SEC). The purity was confirmed by observation of single peak on SEC and single band of ~45 KDa on 12% SDS as well as by MALDI-TOF mass spectrometry (Fig. 3A and B). The protein elution volume through SEC corresponded to a 90.2 KDa peak, indicating dimeric nature of LdAI.

SAXS Intensity I(Q) profiles for different concentrations of LdAI were plotted as double logarithmic log I(Q) vs Log Q, indicated lack of aggregation or inter particulate effect in the samples at all concentrations (Fig. 3C). Monodispersity of the samples was confirmed by linear fit in the Guinier region for all the concentrations of the LdAI protein (Fig. 3D). Slope of the linear fit in the Guinier region provide the R_g values for wild type LdAI to be 2.7 nm, similarly R_c value was found to be 1.59, respectively presuming rod-like nature of the scattering particle (Fig. 3D, Supplementary Table 2). From these R_g and R_c values theoretical persistent length (L) of the scattering particle was calculated (where $L = SQRT(12*Rg^2-Rc^2)$) as 7.56 nm. Kratky profiles of SAXS I(Q) plotted as $I(Q)*Q^2$ depicts the globular nature of the protein (Fig. 3E). *P(r)* analysis done by distance distribution function of SAS data analysis (Petoukhov et al., 2012) using indirect Fourier transformation brought forth the D_{max} value to be 8.9 nm, which gives an idea that LdAI attain dimeric state for activity (Fig. 3F, Supplementary Table 2). Additionally, DATMOW(Franke and Svergun, 2009) program was used to calculate the molecular weight of the scattering particles using *P(r)* files (which estimates the molecular weight based on volume correlation V_C), and were found to be very close to the dimeric molecular weight (82.5 kDa). Global shapes of LdAI in solution were computed by SAXS data profiles, SAXS envelope generated were then superimposed on the crystal structure of PfA (Svergun, 1999) (PDB ID 4Q0M) after automated alignment of inertial axes of SAXS based envelopes using *SUPCOMB*(Kozin and Svergun, 2001) (Fig. 3G). The overlaid model matched quite well with the crystal structure of dimeric PfA confirming that LdAI acts as a dimer.

3.4. Modulation of specific activity with temperature and pH

Some asparaginases show an associated glutaminase activity due to similar molecular volumes of L-asparagine and L-glutamine. Interestingly, glutaminase activity in LdAI overwhelmed its asparaginase activity (Supplementary Fig. 2A). It might be therefore possible for *Leishmania* to exploit LdAI for hydrolyzing both the substrates but predominantly L-glutamine as nitrogen source. Thus, all activity measurements and dependence of specific activity on physico-chemical parameters were analyzed in terms of glutaminase property of LdAI. Also, *Leishmania* experiences drastic physico-chemical changes during its digenetic life cycle. During promastigote stage in Sand fly, it is adapted to 300 K and a neutral pH whereas amastigotes reside inside humans at temperature of 310 K and an acidic pH of 5.5. Thus, it was necessary to assess sensitivity of LdAI to different temperatures and pH. Optimal activity of the enzyme was observed between pH 6–8, with decrease in activity below pH 6.0 (Supplementary Fig. 2B). The optimum temperature for LdAI activity was found to be between 30 and 40 °C (Supplementary Fig. 2C).

3.5. Binding and competitive binding of inhibitors with LdAI

3.5.1. Association of inhibitors with LdAI

Apparent dissociation constants for both Asp/Glu and L1 and L2 with LdAI were initially determined by fluorometric titrations (Fig. 4A–D). With increase in concentration of substrate/inhibitor, a gradual decrease in fluorescence intensity was observed. In case of L1 and L2 a concomitant red shift was also observed upon binding. Both L1 and L2 exhibited strong binding with LdAI as indicated by their dissociation constants in the micro molar range (1.6 ± 0.2 and 2.1 ± 0.3 μM, respectively) compared to that of Asp (2.4 ± 0.4 μM) and Glu (11.6 ± 1.3 μM).

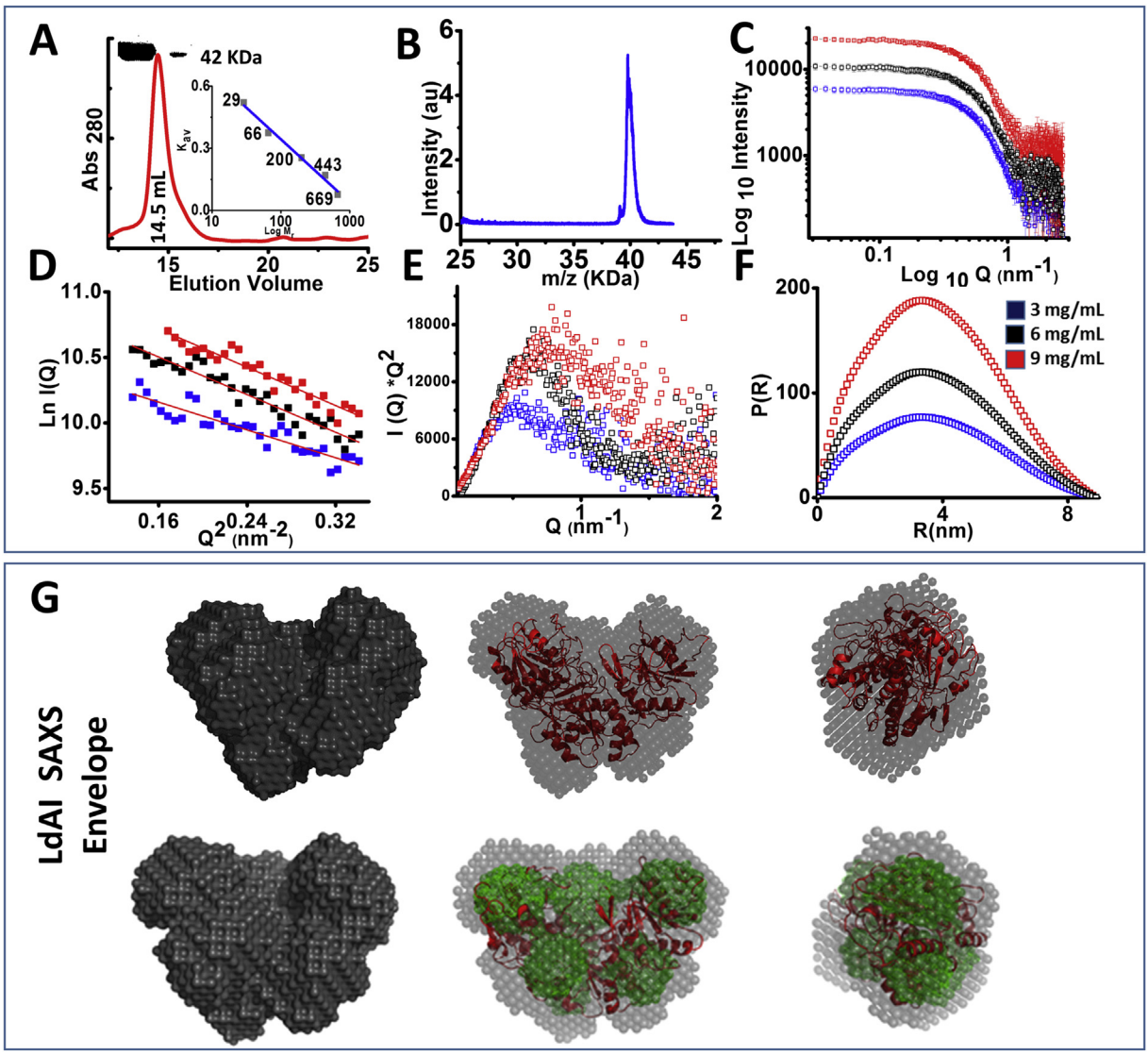

Fig. 3. Purification and Structural characterization of LdAI. (A) Size exclusion chromatography profile of purified LdAI showing single elution peak corresponding to dimeric molecular weight of 91.8 kDa. Insets show SEC standard (Left) and an SDS-PAGE of the eluted peak. (B) MALDI-TOF of purified LdAI. (C) SAXS-based Intensity plots of LdAI protein at different concentrations. (D) Kratky plot showing the globular nature of LdAI protein (E) Linear fit in Guinier region and (F) P(R) plot for the LdAI. (G) Uniform density averaged SAXS models and its overlay over modeled LdAI in different orientations.

ITC studies confirmed the binding affinities obtained previously (Fig. 5 and Table 1). Analysis showed that L-glutamate and L-aspartate had lower apparent binding affinities to LdAI than L1 and L2, indicated through their comparatively lesser free energy of binding (Table 1).

3.5.2. Competitive binding to LdAI

Under physiological environment the binding of L1 and L2 to LdAI will get naturally influenced by the presence of Asp/Glu. To mimic this situation ITC was performed for determining the competitive binding of both the ligands for the active site pocket in the presence of Asp/Glu (Fig. 6). Both L1 and L2 showed roughly 2–4 fold reduction in binding affinity towards LdAI in the presence of Asp/Glu which was also reflected by slight decrease in binding free energy (Table 1). Binding energy analysis on these profiles suggested that the association was enthalpically driven with insignificant positive entropic contributions (Fig. 7). Interestingly, in case of Asp the binding was both enthalpy and entropy driven suggesting contributions of both hydrogen bonding interaction and favorable conformational changes (Fig. 7). In case of binding of L1 and L2 to LdAI similar ΔG values were obtained, although the enthalpic contribution exhibited by L1 was substantially lower than that of L2.

3.6. Effect of inhibitors on enzyme kinetics and protein stability and specificity for LdAI

The competitive inhibition of LdAI by L1 and L2 were further assessed in terms of their modulation of specific activity. The enzyme-inhibitor complex was incubated against varying substrate (Gln) concentrations to determine Michaelis-Menten kinetic parameters (Fig. 8A). Marked changes in kinetic profile of LdAI were observed in the presence of L1 and L2 at saturating binding concentrations (Table 2). Both were found to reduce the catalytic efficiency of LdAI. Ligand binding has often been shown to stabilize proteins. To assess this effect for L1 and L2 on LdAI fluorescence thermal shift (FTS) assay (also known by Differential Scanning Fluorimetry) was performed (Krishna et al., 2013; Niesen et al.,

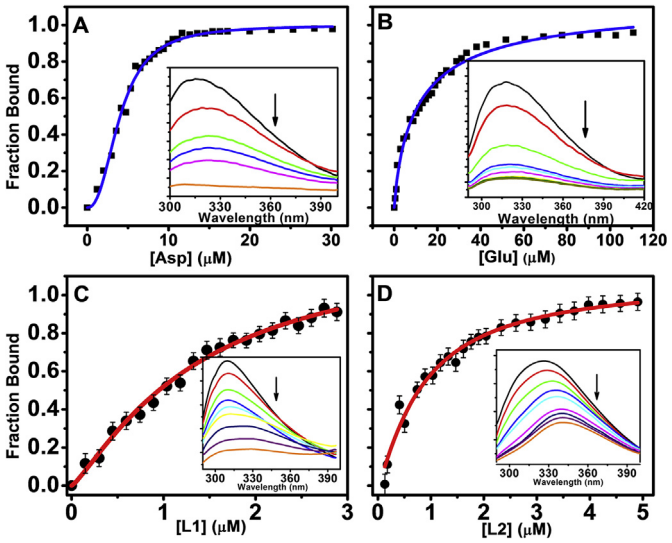

Fig. 4. Fluorescence Titrations. Nonlinear curve fits of fluorescence emission maxima to determine the apparent dissociation constant (K_d) for LdAI with (A) Asp, (B) Glu, (C) L1 and (D) L2, respectively. Insets in each panel show the fluorescence emission spectra (300–400 nm) for the titration of increasing concentration of individual ligands (downward arrow) against LdAI. In each case the LdAI concentration used was 2 μM.

2007). The mid-point of transition/change in fluorescence signal, called the melting temperature (T_m) was determined for LdAI alone and in the presence of inhibitors (Fig. 8B). LdAI showed T_m of 49.4 °C whereas presence of L1 and L2 shifted the T_m of enzyme by ~15 °C (65.1 for L1 and 65.8 for L2 suggesting an overall stabilizing effect. Enzyme activity profiles for our previously characterized enzymes EcAII and PfA remained unaltered in the presence of L1 and L2, signifying specificity of these inhibitors for LdAI only (Supplementary Fig. 3).

3.7. MD simulations of L1 and L2 with LdAI

To gain atomic insights into structural stabilization of LdAI by L1 and L2, all atomic simulations were carried out for 100 ns (Fig. 9). The two monomers of LdAI are stabilized through H-bond between VAL 297 (H) - ASP 118' (OD2) and salt-bridge between ASP 328 (OD1) - HIS 121' (ND1) at dimer interface (Krissinel and Henrick, 2007). We assessed the integrity of these interactions over the simulation period as a measure of structural stability. In simulations of LdAI alone, projection of variations in H-bond vs salt bridge interactions (measured in terms of inter-atomic distance) showed prominent dual distribution along both components (Fig. 9A), suggesting structural fluctuations. These were characterized by species having comparatively higher H-bond (D_{hb}) and salt-bridge (D_{sb}) distance between the atoms. However, in the presence of L1 and L2 only moderate variations were observed along both components (Fig. 9B–C). This was also confirmed through absence of dimer twisting analyzed through angular variations between two monomeric units. Single normal distribution around ~165° angle

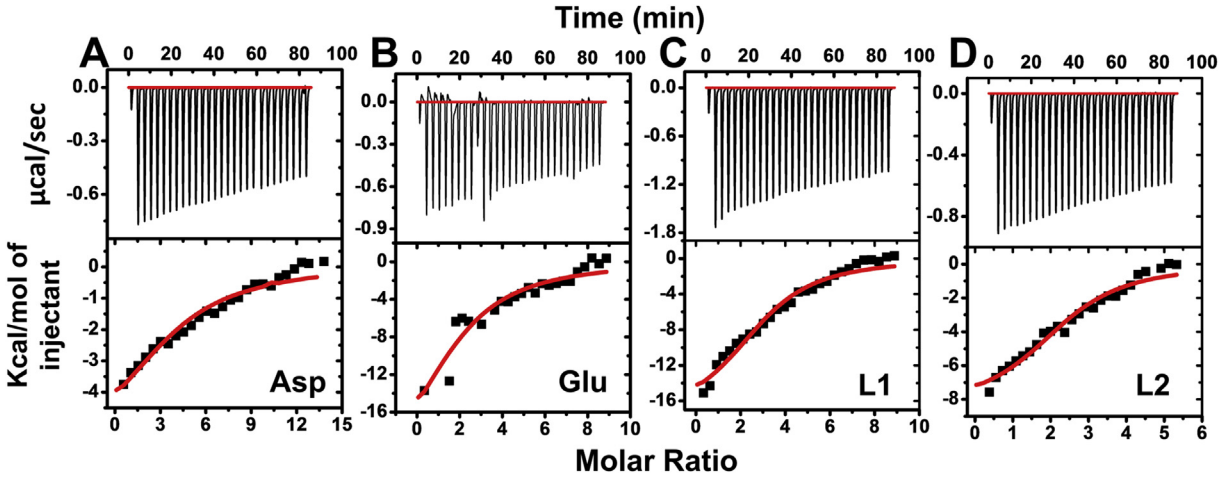

Fig. 5. ITC titrations. Representative ITC profiles for the binding of (A) Asp, (B) Glu, (C) L1 and (D) L2, respectively with LdAI at 298 K. The upper panels in the ITC profiles show the heat of association for ligand-protein interactions. The lower panels show the heat exchanged per mole of injectant as a function of molar ratio of ligand to protein. Solid red lines represent the fitted isotherms obtained using "one set of sites" binding model after subtracting appropriate controls. In each case the LdAI concentration used was 3 μM. (For interpretation of the references to colour in this figure legend, the reader is referred to the web version of this article.)

Table 1
Thermodynamic parameters obtained from ITC experiments.

System	N (Drug/LdAI)	K_d (μM)	ΔH (kcal/mol)	TΔS (kcal/mol)	ΔG (kcal/mol)
LdAI + Asp	4.0 ± 0.7	7.7	−6.34 ± 0.3	0.64	−6.98
LdAI + Glu	2.14 ± 0.6	5.0	−25.6 ± 1.1	−18.38	−7.22
LdAI + L1	2.71 ± 0.121	1.05	−8.41 ± 0.6	−0.4	−8.02
LdAI + L2	2.67 ± 0.193	1.2	−17.96 ± 2.1	−9.95	−8.01
L1+(LdAI + Asp)	1.28 ± 0.0583	2.4	−9.58 ± 0.4	−2.09	−7.49
L1+(LdAI + Glu)	3.97 ± 0.168	2.0	−12.41 ± 1.4	−4.62	−7.79
L2+(LdAI + Asp)	3.50 ± 1.2	5.2	−17.25 ± 1.3	−10.08	−7.17
L2+(LdAI + Glu)	3.59 ± 0.178	2.5	−16.53 ± 1.2	−8.88	−7.65

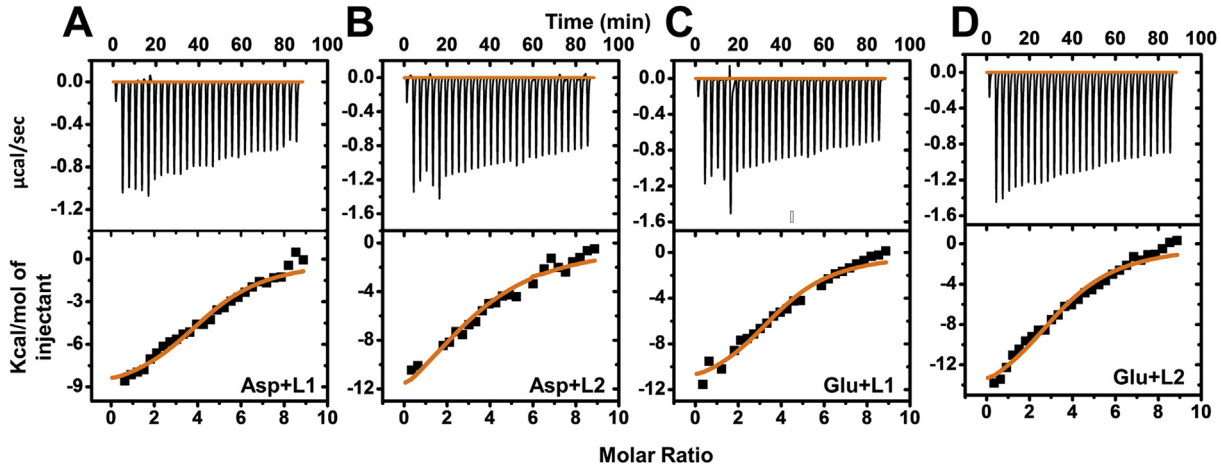

Fig. 6. Competitive ITC titrations. Representative ITC profiles for the binding of (A) L1 and (B) L2 with LdAI-Asp complex (C) L1 and (D) L2 with LdAI-Glu complex at 298 K. Upper panels in the ITC profiles show the heat of association for ligand-macromolecule interactions. The lower panels show the heat exchanged per mole of injectant as a function of molar ratio of ligand to macromolecule. Solid orange lines represent the fitted isotherms obtained using competitive binding model after subtracting appropriate controls. In each case the LdAI concentration used was 3 µM. (For interpretation of the references to colour in this figure legend, the reader is referred to the web version of this article.)

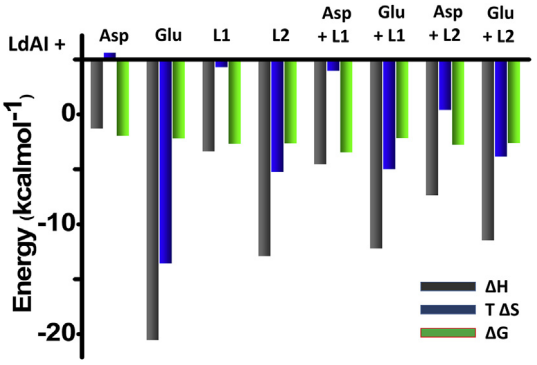

Fig. 7. Binding energetics of ITC and competitive ITC experiments. The enthalpy change for the ligand-macromolecule association is denoted by ΔH, the entropy factor is denoted by TΔS and the free energy change for the interaction is denoted by ΔG in each case.

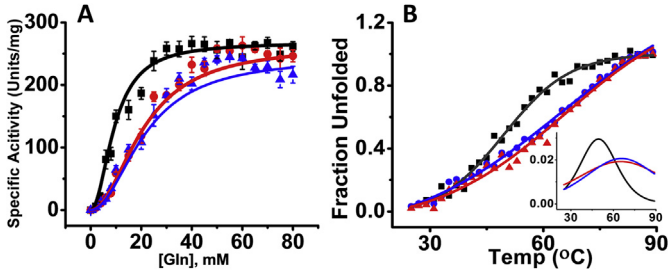

Fig. 8. Kinetic parameters and thermal stability in presence of inhibitors. (A) Kinetics of the Gln conversion by LdAI (Black) and in presence of L1 (Red) and L2 (Orange LdAI concentration used was 5 µM. (B) FTS assay to determine melting temperature (T_m) of LdAI alone (Black) and in presence of L1 (Red) and L2 (blue). Insets show first derivatives of T_m curves. The LdAI concentration used was 2 µM. (For interpretation of the references to colour in this figure legend, the reader is referred to the web version of this article.)

(inter-monomer angle) was observed for both L1 and L2 bound LdAI complexes. Interestingly for apo system, bimodal distribution around ~170° and ~150° was observed (Fig. 9A–C (insets)) indicating twisting of both monomers. Finally, free energy landscapes were constructed for the respective systems projected as function of macroscopic parameters as overall backbone root mean square deviation (RMSD) and gyration radius (Fig. 9D–F). In the presence of L1 and L2, the energy landscape became more scattered and drifted towards an entirely different conformational space. In the presence of L1, the lowest free energy basin was confined to similar conformational subspace as LdAI but we could anticipate formation of alternate basins with more simulation time period. However in presence of L2, the lowest free energy basin corresponded closely to starting structure of LdAI inferred through species with moderate fluctuations in RMSD and Rg. The simulated LdAI alone showed comparatively higher RMSD (3.5 Å) while in presence of L1 and L2 it showed minimal structural RMSD (2.2 Å and 2.9 Å) compared to original starting model (Inset).

3.8. Effects of L1 and L2 on wild-type and LdAI over-expressing parasites

Survival of wild type and LdAI overexpressing *L. donovani* was studied upon treatment with varying concentrations of inhibitors L1 and L2 and to AmB. Percentage survival was calculated after incubation for 48, 72 and 96 h. As a representative, survival analysis after 72 h is shown in Fig. 10. Both L1 and L2 showed dose-dependent inhibition on the growth of wild type *L. donovani*.The IC_{50} for L1 and L2 was comparatively higher than AmB. However, these dose-dependent inhibitory effects of the inhibitors were moderated by LdAI over-expressing *L. donovani*, at all sampling intervals. The IC_{50} for L1 and L2 also quadrupled in LdAI over-expressing parasites. (Supplementary Table 1).

3.9. Neurotoxicity and hepatotoxicity of inhibitors

Previously screened inhibitors were tested for possible neurotoxic and hepatotoxic behaviors at concentrations used to test their effectiveness against *Leishmania* promastigotes. Mouse neuroblastoma (N2a) cells and Human embryonic kidney (HEK 293) cells were employed for toxicity assessments. Both inhibitors did not show any marked effects on cell viability except only for L2 which showed nearly 10% reduction at higher concentrations (Supplementary Fig. 6).

Table 2
Kinetic Constants for LdAI with Gln as substrate and in presence of two inhibitors L1 and L2.

System	Km (mM)	Vmax	Kcat (min^{-1})	Catalytic Efficiency ($min^{-1}M^{-1}$)
Gln + LdAI	9.5 ± 0.8	267.9 ± 7.6	26,790 ± 760	2.82
Gln+(LdAI + L1)	21 ± 2.3	263 ± 18.3	26,300 ± 80	1.25
Gln+(LdAI + L2)	25.6 ± 5.8	244.7 ± 36.3	24,470 ± 3630	0.95

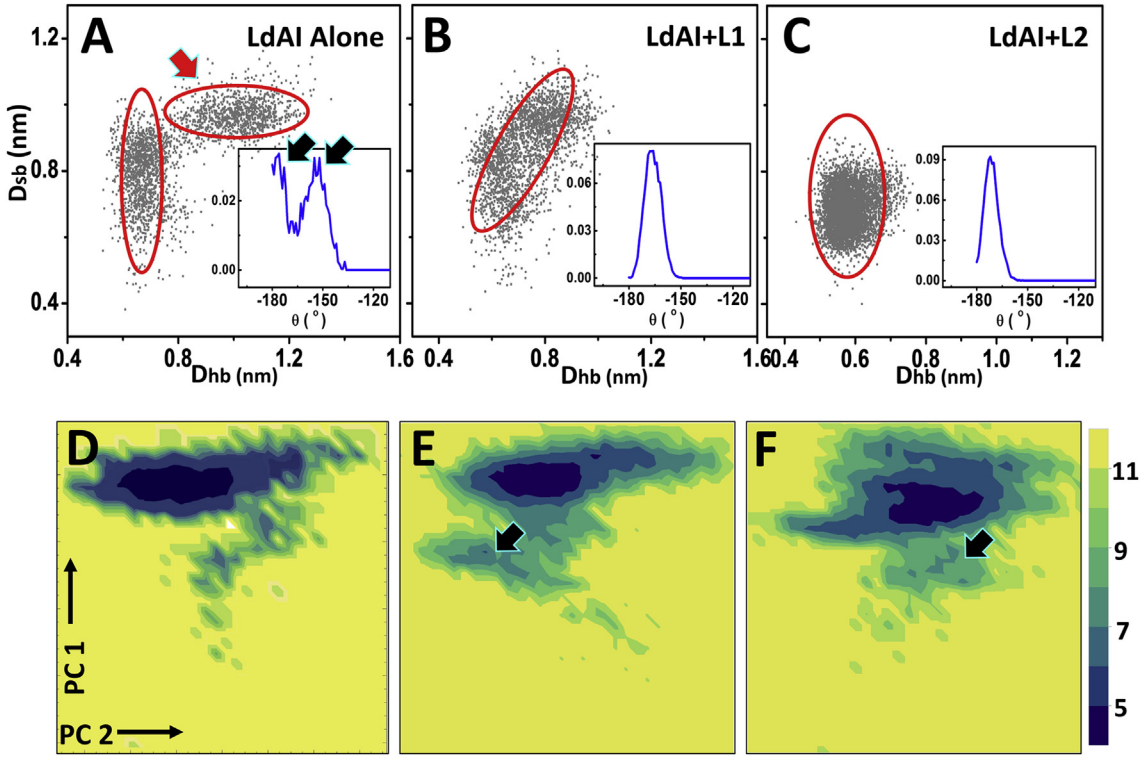

Fig. 9. Projections of MD simulations for LdAI alone and in bound state with L1 and L2. (A–C) Distributions of H-bond (D_{hb}) between VAL 297 (H) - ASP 118' (OD2) and salt-bridge distance (D_{sb}) between ASP 328 (OD1) - HIS 121' (ND1) at LdAI dimer interface averaged over whole 100 ns trajectory for LdAI alone (A, red arrows point an alternate distribution indicating disruption of H-bond and salt-bridge at interface) and in presence of L1 and L2 (B–C) bound at oppositely oriented active sites. Insets show inter-chain angle distribution averaged over whole trajectory (Blue arrows indicate bimodal distribution). (D) Free energy landscapes (Kcal/mol) projected as function of two macroscopic principal components (Gyration radius (PC1) and Backbone RMSD (PC2)) for LdAI alone and (E–F) in presence of L1 and L2. Arrows indicate possibility of other alternate low energy states close to starting model. (For interpretation of the references to colour in this figure legend, the reader is referred to the web version of this article.)

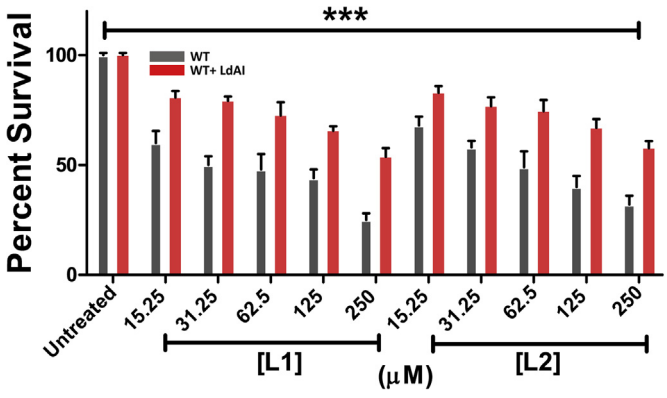

Fig. 10. Cytotoxicity studies. Cytotoxic effects of inhibitors L1 and L2 probed though MTT assay after 72 h on cultured *L. donovani* wild type (Grey) and LdAI transfected promastigotes (Red). *, $p < 0.05$; **, $p < 0.01$; ***, $p < 0.001$ by two way ANOVA using GraphPad Prism 5.0 on three independent data sets. (For interpretation of the references to colour in this figure legend, the reader is referred to the web version of this article.)

4. Discussions

Multiple drug resistance have inclined researchers to explore nodal metabolic networks through genome-wide analysis (Skuce et al., 2010; Laing et al., 2010; Singh et al., 2014; Lakshmi et al., 2014; Biyani and Madhubala, 2012) for identifying key metabolites/genes essential for parasite survival. In case of AmB resistance in *Leishmania* spp., many reports on interplay of one or more factors as increased expression of MDR1, upregulation of tryparedoxin cascade and ABC transporters etc. have been highlighted and supported through direct experimental evidences from AmB resistant clinical isolates (Purkait et al., 2012). However, much of the previous efforts were focused on late-phase acquired resistance and as an immediate effect how the pathogen responds to the initial AmB onslaught had often been overlooked. Backed by thorough experimental support we identified LdAI as a crucial metabolic enzyme involved in conferring early resistance to AmB.

We propose this based on increased expression of LdAI upon exposing L. *donovani* parasites to AmB. To support our initial observations, both LdAI over-expressing promastigotes and axenic amastigotes of *L. donovani* were challenged with AmB, where again increased tolerance to drug and therefore better survival of

transfected strains was observed compared to wild type (non-transfected) strains (Fig. 1). This effect persisted even after three days exposure to all test concentrations of AmB, emphasizing the significance of LdAI in conferring drug resistance phenotype. Previous reports have mentioned the importance of membrane ergosterol content in conferring AmB resistance phenotype (Purkait et al., 2012; Saha et al., 1986). The enzyme reported to be malfunctioning/absent in the resistant phenotypes is S-adenosyl-L-methionine-C24 Δ-sterol methyl transferase (SCMT) responsible for synthesis of ergosterol from cholesta-5,7,24-trien-3β-ol (Pourshafie et al., 2004; Brotherton et al., 2014). In another report the importance of AmB mediated membrane pore formation, K^+ leakage and concomitant downregulation of H1A-2 P-type H^+ -ATPase has been proposed (Brotherton et al., 2014). However transfection experiments failed to restore WT phenotype. In our study, we not only found significant overexpression of LdAI in AmB treated *L. donovani* but also could demonstrate growth restoration upon transfection with LdAI.

We also propose that in a state where H^+-ATPase is down-regulated, the cytoplasmic over-expression of LdAI could neutralize the proton influx induced by AmB-mediated aqueous pores, thus maintaining the much required neutral intracellular environment. Once the parasite survives the initial AmB onslaught, other protective measures, as reported earlier, might take over to confer late phase persistent resistance.

The resistance mechanisms prompted us to look for metabolic role of LdAI in wild type growing parasites. Search for L-asparaginases among various pathogenic microorganisms highlighted the conspicuous presence of L-asparaginase in *L. donovani, M. tuberculosis, S. typhi, H. pylori and T. cruzi*. Interestingly, all these organisms either need to survive inside acidic environment of hosts or modulate their immune responses through asparagine metabolism. Sequence analysis of these L-asparaginases displayed conservation of crucial catalytic residues and negligible identity with human L-asparaginase (Fig. 2B), thereby also projecting this enzyme as attractive metabolic target against leishmaniasis. Unfortunately, we could not make null mutant of this enzyme, so we opted to rational design of its specific inhibitors, for which we first resorted to complete characterization using various bioinformatics and biochemical approaches. In the absence of structural information, the SEC and SAXS analysis validated our earlier proposed dimeric model for LdAI and established that it is structurally similar to *P. furiosus* L-asparaginase (Bansal et al., 2010; Garg et al., 2015; Tomar et al., 2016) and earlier studied cytoplasmic L-asparaginases (Yun et al., 2007). We then screened out two potential inhibitors L1 and L2 based on structural information of the enzyme active site and their similarity to substrate. Both inhibitors showed higher binding affinities compared to the products Asp/Glu. The effects could be explained in terms of number of H-bond donors (HBD) and acceptors (HBA) between competing molecules. The inhibitors possessed 5 HBD and up to 8 HBA groups compared to Asp/Glu which had 3-5 of both HBD/HBA groups. The binding of inhibitors was mostly enthalpy driven with corresponding negative entropic contributions (Fig. 7). However, enthalpy contribution in binding of L2 was higher than L1. This could be due to higher H-bond interactions of L2 with seven residues of the active pocket namely Thr 38, Leu 49, His 192, Asp 85 and Ser 87, Asp 118 and Met 144 (Singh et al., 2015). However, L1 interactions mediated through single H-bond with Thr 38 and five other H-bonds with four residues viz. Leu 49, Ser86, Met41 and Asp85 with its indole ring. Similarly, negative entropic contributions (unfavorable conformational change) upon binding of L2 corroborated with fluorescence binding assays where L2 induced greater red shift around λ_{max} (317 nm) while only marginal changes was observed for L1 binding. In cellular milieu, it is expected that molecules with similar physicochemical features would compete for binding at same catalytic site. As the identified compounds were screened on the basis of their affinity with residues of active site of LdAI, their binding affinity can be naturally affected in the presence of substrate or enzyme products giving rise to competition for binding. In line with previously studied competitive binding systems for DNA/proteins (Banerjee et al., 2013, 2014; Lahiri et al., 2012), the binding affinity of both L1 and L2 decreased in the presence of Asp/Glu. The same was also evident through corresponding decrease in binding free energy (~0.2–0.5 kcal/mol) of inhibitors (Table 2). This lower association could be due to inter-molecular competition and conformational remodeling of LdAI upon prior association with Glu/Asp, as observed usually for two competing ligands (ethidium bromide and netropsin binding to DNA (Banerjee et al., 2013) and 5-fluorouracil and cyclophosphamide to bind serum albumin (Thoppil et al., 2016)). In case of competitive binding of L1 and L2, their association was pre-dominated by enthalpy contributions only. Stabilization of LdAI upon binding to inhibitors was proven through FTS assays which could be attributed to formation of extra inter-molecular H-bond network. Understanding of L1 and L2 mediated stabilization of LdAI was attempted through MD simulations. Structural organization of polymeric proteins is known to be stabilized through H-bond/Salt-bridge/cation-pi interactions operating at polymer interface in homo/heteromers (Garg et al., 2015). The oppositely oriented monomers in dimer LdAI was found to be stabilized exclusively through H-bond and salt-bridge interactions at its dimer interface. The simulations at constant temperature of LdAI alone showed angular twisting of individual monomers which could have resulted in disruption of native salt-bridges and H-bonds at the interface (Fig. 9). However in the presence of inhibitors, these interactions remained predominantly intact during the simulations for which angular twisting within the monomers was expectedly not observed. The free energy surfaces not only showed drift in conformational subspace but also showed possibility of other low free energy basins close to initial structure of LdAI indicating the native architectural stabilization by L1 and L2. Overall the simulation projections can be extended to L1 and L2 induced stabilization of LdAI where native protein interactions were predominantly intact leading to increased T_m (Fig. 8).

Finally, we observed dose dependent effects of both inhibitors on cultured parasites. Expectedly, the IC_{50}'s of L1 and L2 were comparatively higher than reference drug, AmB. As hypothesized that LdAI could not be sole contributor in nitrogen metabolism, the transaminases and synthases could co-operate within the same sub-cellular compartment to replenish important reaction intermediates. Further evidence was garnered from STRING database which predicted functional association of LdAI with key enzymes involved in aspartate and arginine and purine metabolism of parasite (Fig. 2D). Two of these key enzymes (both cytosolic); arginosuccinate synthase (Sardar et al., 2016; Lakhal-Naouar et al., 2012) involved in arginine synthesis and adenonylate synthetase in salvage pathway for purine biosynthesis were predicted to be strongly interacting (90% confidence) with LdAI. Both enzymes had been proved earlier in synthesis of arginosuccinate (ATP dependent) and adenonylate (GTP dependent) using Asp as substrate (Saunders et al., 2011). Functional inactivation of these enzymes had been shown to induce growth and infectivity deficits in parasite (Lakhal-Naouar et al., 2012; Sardar et al., 2016; Manhas et al., 2014). Thus, it does reflect combinatorial inter-dependence of these pathways, the knowledge of which could be integrated together for effectively targeting nitrogen metabolism of the parasite. Apparently, we also could not exclude possibility of off-targeting effects by the inhibitors with the proteome of parasite. Fortunately, this undesired possibility was ruled out using an over-expression system as LdAI over-expressing parasites showed

resistance to inhibitory effects at all concentrations of both the inhibitors, observed through ~20% increase in survival rate (Fig. 10). Moreover, another probable L-asparaginase (LDBPK_364,650) has also been identified based on genome analysis. However, its overexpression in parasites failed to confer any survival advantage on AmB exposure (data not shown), validating key role of LdAI in providing early tolerance to the drug.

In line with earlier reports of Glu/Asp metabolism proven crucial for TCA cycle anaplerosis, our results conclusively establish L-asparaginase of *L. donovani* as one of the key metabolic enzyme for early protective response to Amphotericin B, the mainstay therapeutic employed for visceral leishmaniasis. Collectively, this study provides molecular insights into knowledge based, rational targeting of metabolic networks and understanding chemoresistance with an aim to develop better therapeutics.

Author contributions

BK and JS designed this study. All authors contributed in analysis of data. JS, SPSY and IK performed experiments. BK and JS wrote the manuscript. All authors provide critical reviews and contributed in finalizing the manuscript.

Competing financial interests

The authors declare no competing financial interests.

Acknowledgements

This work received infrastructural support from IIT Delhi, CSIR IMTECH and NIPER Hajipur. JS and SPSY acknowledge fellowship support from IIT Delhi and DST-INSPIRE, India respectively. The authors are indebted to Prof. Subrata Banerjee (Biophysics and Structural Genomics Division, SINP Kolkata) for permissions to carry ITC experiments and the Intramural Funding from Department of Atomic Energy, Govt. of India. We also thank Prof. Dipak Dasgupta and Dr. Amrita Banerjee for ITC related discussions and troubleshooting. We are thankful to Rishibha Sachdev for critical review of manuscript and technical discussions. Authors thank the IIT Delhi HPC facility for computational resources.

Appendix A. Supplementary data

Supplementary data related to this article can be found at https://doi.org/10.1016/j.ijpddr.2017.09.003.

References

Alvar, J., Velez, I.D., Bern, C., Herrero, M., Desjeux, P., Cano, J., Jannin, J., den Boer, M., Team, W.H.O.L.C., 2012. Leishmaniasis worldwide and global estimates of its incidence. PLoS One 7, e35671.

Anderson, S.A., Mukkada, A.J., 1994. Biochemical and immunochemical characterization of a P-type ATPase from Leishmania donovani promastigote plasma membrane. Biochim. Biophys. Acta 1195, 71–80.

Arning, M., Kliche, K.O., Heer-Sonderhoff, A.H., Wehmeier, A., 1995. Infusion-related toxicity of three different amphotericin B formulations and its relation to cytokine plasma levels. Mycoses 38, 459–465.

Banerjee, A., Singh, J., Dasgupta, D., 2013. Fluorescence spectroscopic and calorimetry based approaches to characterize the mode of interaction of small molecules with DNA. J. Fluoresc. 23, 745–752.

Banerjee, A., Majumder, P., Sanyal, S., Singh, J., Jana, K., Das, C., Dasgupta, D., 2014. The DNA intercalators ethidium bromide and propidium iodide also bind to core histones. FEBS Open Bio 4, 251–259.

Bansal, S., Gnaneswari, D., Mishra, P., Kundu, B., 2010. Structural stability and functional analysis of L-asparaginase from Pyrococcus furiosus. Biochem. (Mosc) 75, 375–381.

Bellocchio, S., Gaziano, R., Bozza, S., Rossi, G., Montagnoli, C., Perruccio, K., Calvitti, M., Pitzurra, L., Romani, L., 2005. Liposomal Amphotericin B activates antifungal resistance with reduced toxicity by diverting Toll-like receptor signalling from TLR-2 to TLR-4. J. Antimicrob. Chemother. 55, 214–222.

Beverley, S.M., Clayton, C.E., 1993. Transfection of Leishmania and trypanosoma brucei by electroporation. Methods Mol. Biol. 21, 333–348.

Biyani, N., Madhubala, R., 2012. Quantitative proteomic profiling of the promastigotes and the intracellular amastigotes of Leishmania donovani isolates identifies novel proteins having a role in Leishmania differentiation and intracellular survival. Biochim. Biophys. Acta 1824, 1342–1350.

Brotherton, M.C., Bourassa, S., Legare, D., Poirier, G.G., Droit, A., Ouellette, M., 2014. Quantitative proteomic analysis of Amphotericin B resistance in Leishmania infantum. Int. J. Parasitol. Drugs Drug Resist 4, 126–132.

Casgrain, P.A., Martel, C., Mcmaster, W.R., Mottram, J.C., Olivier, M., Descoteaux, A., 2016. Cysteine peptidase B regulates Leishmania mexicana virulence through the modulation of GP63 expression. PLoS Pathog. 12, e1005658.

Chakravarty, J., Sundar, S., 2010. Drug resistance in leishmaniasis. J. Glob. Infect. Dis. 2, 167–176.

Chandra, R., Puri, S.K., 2015. Arteether resistance reversal by ketoconazole/fluconazole in rodent malaria parasite Plasmodium vinckei. Parasitol. Res. 114, 1239–1243.

Cohen, B.E., 2010. Amphotericin B membrane action: role for two types of ion channels in eliciting cell survival and lethal effects. J. Membr. Biol. 238, 1–20.

Croft, S.L., Sundar, S., Fairlamb, A.H., 2006. Drug resistance in leishmaniasis. Clin. Microbiol. Rev. 19, 111–126.

Cull, B., Prado Godinho, J.L., Fernandes Rodrigues, J.C., Frank, B., Schurigt, U., Williams, R.A., Coombs, G.H., Mottram, J.C., 2014. Glycosome turnover in Leishmania major is mediated by autophagy. Autophagy 10, 2143–2157.

Desjeux, P., 2004. Leishmaniasis: current situation and new perspectives. WHO 2017 Comp. Immunol. Microbiol. Infect. Dis. 27, 305–318.

Faria, J., Loureiro, I., Santarem, N., Macedo-Ribeiro, S., Tavares, J., Cordeiro-da-Silva, A., 2016. Leishmania infantum asparagine synthetase a is dispensable for parasites survival and infectivity. PLoS Negl. Trop. Dis. 10, e0004365.

Franke, D., Svergun, D.I., 2009. DAMMIF, a program for rapid ab-initio shape determination in small-angle scattering. J. Appl. Crystallogr. 42, 342–346.

Garg, D.K., Tomar, R., Dhoke, R.R., Srivastava, A., Kundu, B., 2015. Domains of Pyrococcus furiosus L-asparaginase fold sequentially and assemble through strong intersubunit associative forces. Extremophiles 19, 681–691.

Gilleard, J.S., Beech, R.N., 2007. Population genetics of anthelmintic resistance in parasitic nematodes. Parasitology 134, 1133–1147.

Gouzy, A., Larrouy-Maumus, G., Bottai, D., Levillain, F., Dumas, A., Wallach, J.B., Caire-Brandli, I., de Chastellier, C., Wu, T.D., Poincloux, R., Brosch, R., Guerquin-Kern, J.L., Schnappinger, D., Sorio de Carvalho, L.P., Poquet, Y., Neyrolles, O., 2014. Mycobacterium tuberculosis exploits asparagine to assimilate nitrogen and resist acid stress during infection. PLoS Pathog. 10, e1003928.

Herec, M., Dziubinska, H., Trebacz, K., Morzycki, J.W., Gruszecki, W.I., 2005. An effect of antibiotic Amphotericin B on ion transport across model lipid membranes and tonoplast membranes. Biochem. Pharmacol. 70, 668–675.

Jayaram, H.N., Cooney, D.A., Huang, C.Y., 1986. Interaction between L-aspartic acid and L-asparaginase from Escherichia Coli: binding and inhibition studies. J. Enzyme Inhibition 1, 151–161.

Jiang, S., Anderson, S.A., Winget, G.D., Mukkada, A.J., 1994. Plasma membrane K+/H(+)-ATPase from Leishmania donovani. J. Cell Physiol. 159, 60–66.

Kozin, M.B., Svergun, D.I., 2001. Automated matching of high- and low-resolution structural models. J. Appl. Crystallogr. 34, 33–41.

Krishna, S.N., Luan, C.H., Mishra, R.K., Xu, L., Scheidt, K.A., Anderson, W.F., Bergan, R.C., 2013. A fluorescence-based thermal shift assay identifies inhibitors of mitogen activated protein kinase kinase 4. PLoS One 8, e81504.

Krissinel, E., Henrick, K., 2007. Inference of macromolecular assemblies from crystalline state. J. Mol. Biol. 372, 774–797.

Kullas, A.L., Mcclelland, M., Yang, H.J., Tam, J.W., Torres, A., Porwollik, S., Mena, P., Mcphee, J.B., Bogomolnaya, L., Andrews-Polymenis, H., Van der Velden, A.W., 2012. L-asparaginase II produced by Salmonella typhimurium inhibits T cell responses and mediates virulence. Cell Host Microbe 12, 791–798.

Lahiri, S., Takao, T., Devi, P.G., Ghosh, S., Ghosh, A., Dasgupta, A., Dasgupta, D., 2012. Association of aureolic acid antibiotic, chromomycin A3 with Cu2+ and its negative effect upon DNA binding property of the antibiotic. Biometals 25, 435–450.

Laing, S.T., Ivens, A., Laing, R., Ravikumar, S., Butler, V., Woods, D.J., Gilleard, J.S., 2010. Characterization of the xenobiotic response of Caenorhabditis elegans to the anthelmintic drug albendazole and the identification of novel drug glucoside metabolites. Biochem. J. 432, 505–514.

Lakhal-Naouar, I., Jardim, A., Strasser, R., Luo, S., Kozakai, Y., Nakhasi, H.L., Duncan, R.C., 2012. Leishmania donovani argininosuccinate synthase is an active enzyme associated with parasite pathogenesis. PLoS Negl. Trop. Dis. 6, e1849.

Lakshmi, B.S., Wang, R., Madhubala, R., 2014. Leishmania genome analysis and high-throughput immunological screening identifies tuzin as a novel vaccine candidate against visceral leishmaniasis. Vaccine 32, 3816–3822.

Lu, P., Ma, D., Chen, Y., Guo, Y., Chen, G.Q., Deng, H., Shi, Y., 2013. L-glutamine provides acid resistance for Escherichia coli through enzymatic release of ammonia. Cell Res. 23, 635–644.

Luque-Ortega, J.R., Saugar, J.M., Chiva, C., Andreu, D., Rivas, L., 2003. Identification of new leishmanicidal peptide lead structures by automated real-time monitoring of changes in intracellular ATP. Biochem. J. 375, 221–230.

Manhas, R., Tripathi, P., Khan, S., Sethu Lakshmi, B., Lal, S.K., Gowri, V.S., Sharma, A., Madhubala, R., 2014. Identification and functional characterization of a novel bacterial type asparagine synthetase A: a tRNA synthetase paralog from Leishmania donovani. J. Biol. Chem. 289, 12096–12108.

Mateos-Gonzalez, F., Sundstrom, L.F., Schmid, M., Bjorklund, M., 2015. Rapid evolution of parasite resistance in a warmer environment: insights from a Large scale field experiment. Plos One 10.
Matsuo, K., Hotokezaka, H., Ohara, N., Fujimura, Y., Yoshimura, A., Okada, Y., Hara, Y., Yoshida, N., Nakayama, K., 2006. Analysis of Amphotericin B-induced cell signaling with chemical inhibitors of signaling molecules. Microbiol. Immunol. 50, 337–347.
Mcconville, M.J., 2016. Metabolic crosstalk between Leishmania and the macrophage host. Trends Parasitol. 32, 666–668.
Mcconville, M.J., Naderer, T., 2011. Metabolic pathways required for the intracellular survival of Leishmania. Annu. Rev. Microbiol. 65, 543–561.
Mesa-Arango, A.C., Scorzoni, L., Zaragoza, O., 2012. It only takes one to do many jobs: Amphotericin B as antifungal and immunomodulatory drug. Front. Microbiol. 3, 286.
Mihu, M.R., Pattabhi, R., Nosanchuk, J.D., 2014. The impact of antifungals on toll-like receptors. Front. Microbiol. 5, 99.
Morales, M.A., Watanabe, R., Laurent, C., Lenormand, P., Rousselle, J.C., Namane, A., Spath, G.F., 2008. Phosphoproteomic analysis of Leishmania donovani pro- and amastigote stages. Proteomics 8, 350–363.
Morales, M.A., Watanabe, R., Dacher, M., Chafey, P., Osorio Y Fortea, J., Scott, D.A., Beverley, S.M., Ommen, G., Clos, J., Hem, S., Lenormand, P., Rousselle, J.C., Namane, A., Spath, G.F., 2010. Phosphoproteome dynamics reveal heat-shock protein complexes specific to the Leishmania donovani infectious stage. Proc. Natl. Acad. Sci. U. S. A. 107, 8381–8386.
Moreno, M.A., Abramov, A., Abendroth, J., Alonso, A., Zhang, S., Alcolea, P.J., Edwards, T., Lorimer, D., Myler, P.J., Larraga, V., 2014. Structure of tyrosine aminotransferase from Leishmania infantum. Acta Crystallogr. F. Struct. Biol. Commun. 70, 583–587.
Mukherjee, A.K., Gupta, G., Bhattacharjee, S., Guha, S.K., Majumder, S., Adhikari, A., Bhattachrya, P., Majumdar, S.B., Majumdar, S., 2010. Amphotericin B regulates the host immune response in visceral leishmaniasis: reciprocal regulation of protein kinase C isoforms. J. Infect. 61, 173–184.
Naderer, T., Mcconville, M.J., 2011. Intracellular growth and pathogenesis of Leishmania parasites. Essays Biochem. 51, 81–95.
Niesen, F.H., Berglund, H., Vedadi, M., 2007. The use of differential scanning fluorimetry to detect ligand interactions that promote protein stability. Nat. Protoc. 2, 2212–2221.
Nowicki, C., Cazzulo, J.J., 2008. Aromatic amino acid catabolism in trypanosomatids. Comp. Biochem. Physiol. A Mol. Integr. Physiol. 151, 381–390.
Palacios, J., Serrano, R., 1978. Proton permeability induced by polyene antibiotics. A plausible mechanism for their inhibition of maltose fermentation in yeast. FEBS Lett. 91, 198–201.
Pentikainen, U., Shaw, K.E., Senthilkumar, K., Woods, C.J., Mulholland, A.J., 2009. Lennard-jones parameters for B3LYP/CHARMM27 QM/MM modeling of nucleic acid bases. J. Chem. Theory Comput. 5, 396–410.
Petoukhov, M.V., Franke, D., Shkumatov, A.V., Tria, G., Kikhney, A.G., Gajda, M., Gorba, C., Mertens, H.D., Konarev, P.V., Svergun, D.I., 2012. New developments in the ATSAS program package for small-angle scattering data analysis. J. Appl. Crystallogr. 45, 342–350.
Pourshafie, M., Morand, S., Virion, A., Rakotomanga, M., Dupuy, C., Loiseau, P.M., 2004. Cloning of S-adenosyl-L-methionine:C-24-Delta-sterol-methyltransferase (ERG6) from Leishmania donovani and characterization of mRNAs in wild-type and Amphotericin B-Resistant promastigotes. Antimicrob. Agents Chemother. 48, 2409–2414.
Purkait, B., Kumar, A., Nandi, N., Sardar, A.H., Das, S., Kumar, S., Pandey, K., Ravidas, V., Kumar, M., De, T., Singh, D., Das, P., 2012. Mechanism of Amphotericin B resistance in clinical isolates of Leishmania donovani. Antimicrob. Agents Chemother. 56, 1031–1041.
Saha, A.K., Mukherjee, T., Bhaduri, A., 1986. Mechanism of action of Amphotericin B on Leishmania donovani promastigotes. Mol. Biochem. Parasitol. 19, 195–200.
Sapay, N., Tieleman, D.P., 2011. Combination of the CHARMM27 force field with united-atom lipid force fields. J. Comput. Chem. 32, 1400–1410.
Sardar, A.H., Jardim, A., Ghosh, A.K., Mandal, A., Das, S., Saini, S., Abhishek, K., Singh, R., Verma, S., Kumar, A., DAS, P., 2016. Genetic manipulation of Leishmania donovani to explore the involvement of argininosuccinate synthase in oxidative stress management. PLoS Negl. Trop. Dis. 10, e0004308.
Sau, K., Mambula, S.S., Latz, E., Henneke, P., Golenbock, D.T., Levitz, S.M., 2003. The antifungal drug Amphotericin B promotes inflammatory cytokine release by a Toll-like receptor- and CD14-dependent mechanism. J. Biol. Chem. 278, 37561–37568.
Saunders, E.C., Ng, W.W., Chambers, J.M., Ng, M., Naderer, T., Kromer, J.O., Likic, V.A., Mcconville, M.J., 2011. Isotopomer profiling of Leishmania mexicana promastigotes reveals important roles for succinate fermentation and aspartate uptake in tricarboxylic acid cycle (TCA) anaplerosis, glutamate synthesis, and growth. J. Biol. Chem. 286, 27706–27717.
Saunders, G.I., Wasmuth, J.D., Beech, R., Laing, R., Hunt, M., Naghra, H., Cotton, J.A., Berriman, M., Britton, C., Gilleard, J.S., 2013. Characterization and comparative analysis of the complete Haemonchus contortus beta-tubulin gene family and implications for benzimidazole resistance in strongylid nematodes. Int. J. Parasitol. 43, 465–475.
Scotti, C., Sommi, P., Pasquetto, M.V., Cappelletti, D., Stivala, S., Mignosi, P., Savio, M., Chiarelli, L.R., Valentini, G., Bolanos-Garcia, V.M., Merrell, D.S., franchini, S., Verona, M.L., Bolis, C., Solcia, E., Manca, R., Franciotta, D., Casasco, A., Filipazzi, P., Zardini, E., Vannini, V., 2010. Cell-cycle inhibition by Helicobacter pylori L-asparaginase. PLoS One 5, e13892.
Sereno, D., Lemesre, J.L., 1997. Axenically cultured amastigote forms as an in vitro model for investigation of antileishmanial agents. Antimicrob. Agents Chemother. 41, 972–976.
Shibayama, K., Takeuchi, H., Wachino, J., Mori, S., Arakawa, Y., 2011. Biochemical and pathophysiological characterization of Helicobacter pylori asparaginase. Microbiol. Immunol. 55, 408–417.
Sigurskjold, B.W., 2000. Exact analysis of competition ligand binding by displacement isothermal titration calorimetry. Anal. Biochem. 277, 260–266.
Singh, A.K., Roberts, S., Ullman, B., Madhubala, R., 2014. A quantitative proteomic screen to identify potential drug resistance mechanism in alpha-difluoromethylornithine (DFMO) resistant Leishmania donovani. J. Proteomics 102, 44–59.
Singh, J., Srivastava, A., Jha, P., Sinha, K.K., Kundu, B., 2015. L-Asparaginase as a new molecular target against leishmaniasis: insights into the mechanism of action and structure-based inhibitor design. Mol. Biosyst. 11, 1887–1896.
Skuce, P., Stenhouse, L., Jackson, F., Hypsa, V., Gilleard, J., 2010. Benzimidazole resistance allele haplotype diversity in United Kingdom isolates of Teladorsagia circumcincta supports a hypothesis of multiple origins of resistance by recurrent mutation. Int. J. Parasitol. 40, 1247–1255.
Solanki, A.K., Rathore, Y.S., Badmalia, M.D., Dhoke, R.R., Nath, S.K., Nihalani, D., Ashish, 2014. Global shape and ligand binding efficiency of the HIV-1-neutralizing antibodies differ from those of antibodies that cannot neutralize HIV-1. J. Biol. Chem. 289, 34780–34800.
Svergun, D.I., 1999. Restoring low resolution structure of biological macromolecules from solution scattering using simulated annealing. Biophys. J. 76, 2879–2886.
Thoppil, A.A., Choudhary, S., Kishore, N., 2016. Competitive binding of anticancer drugs 5-fluorouracil and cyclophosphamide with serum albumin: calorimetric insights. Biochim. Biophys. Acta 1860, 917–929.
Tomar, R., Sharma, P., Srivastava, A., Bansal, S., Ashish, Kundu, B., 2016. Structural and functional insights into an archaeal L-asparaginase obtained through the linker-less assembly of constituent domains. Corrigendum. Acta Crystallogr. D. Struct. Biol. 72, 180.
Tsigankov, P., Gherardini, P.F., Helmer-Citterich, M., Spath, G.F., Myler, P.J., Zilberstein, D., 2014. Regulation dynamics of Leishmania differentiation: deconvoluting signals and identifying phosphorylation trends. Mol. Cell Proteomics 13, 1787–1799.
van den bogaart, E., Schoone, G.J., England, P., Faber, D., Orrling, K.M., Dujardin, J.C., Sundar, S., Schallig, H.D., Adams, E.R., 2014. Simple colorimetric trypanothione reductase-based assay for high-throughput screening of drugs against Leishmania intracellular amastigotes. Antimicrob. Agents Chemother. 58, 527–535.
van der spoel, D., Lindahl, E., Hess, B., Groenhof, G., Mark, A.E., Berendsen, H.J., 2005. GROMACS: fast, flexible, and free. J. Comput. Chem. 26, 1701–1718.
Venkatesan, Borrmann, S., 2015. Polymorphisms in Plasmodium falciparum chloroquine resistance transporter and multidrug resistance 1 genes: parasite risk factors that affect treatment outcomes for P. falciparum malaria after artemether-lumefantrine and artesunate-amodiaquine (vol 91, pg 833, 2014). Am. J. Trop. Med. Hyg. 92, 1084–1084.
Von mering, C., Jensen, L.J., Snel, B., Hooper, S.D., Krupp, M., Foglierini, M., Jouffre, N., Huynen, M.A., Bork, P., 2005. STRING: known and predicted protein-protein associations, integrated and transferred across organisms. Nucleic Acids Res. 33, D433–D437.
Wagner, M.C., Myslinski, J., Pratap, S., Flores, B., Rhodes, G., Campos-bilderback, S.B., Sandoval, R.M., Kumar, S., Patel, M., Ashish, Molitoris, B.A., 2016. Mechanism of increased clearance of glycated albumin by proximal tubule cells. Am. J. Physiol. Ren. Physiol. 310, F1089–F1102.
Yun, M.K., Nourse, A., White, S.W., Rock, C.O., Heath, R.J., 2007. Crystal structure and allosteric regulation of the cytoplasmic Escherichia coli L-asparaginase I. J. Mol. Biol. 369, 794–811.
Zilberstein, D., Blumenfeld, N., Liveanu, V., Gepstein, A., Jaffe, C.L., 1991. Growth at acidic ph induces an amastigote stage-specific protein in Leishmania promastigotes. Mol. Biochem. Parasitol. 45, 175–178.
Zoete, V., Cuendet, M.A., Grosdidier, A., Michielin, O., 2011. SwissParam: a fast force field generation tool for small organic molecules. J. Comput. Chem. 32, 2359–2368.